Dedicated to Academician Aureliu Sandulescu's 80^{th} Anniversary

SUPERASYMMETRIC FISSION VALLEY IN THE ^{238}Pu POTENTIAL LANDSCAPE

M. MIREA

"Horia Hulubei" National Institute for Physics and Nuclear Engineering,
P.O. Box MG-6, Bucharest, Romania
Email: mirea@ifin.nipne.ro

Received September 23, 2011

A superasymmetric fission trajectory for the emission of ^{32}Si from ^{238}Pu is determined by using the minimal action principle. The deformation energy is computed in the frame of the macroscopic-microscopic approach while the inertia is obtained within the cranking approximation. The nuclear shape parametrization takes into account five degrees of freedom associated to the elongation, necking, mass asymmetry and deformations of nascent fragments. The single particle energies and the nucleon wave functions are obtained within the superasymmetric Woods-Saxon two center shell model. Our calculations confirm that the cluster decay follows a potential magic valley, starting from the ground state of the parent and reaching a configuration of two touching nuclei at scission.

Key words: Cluster decay, Two center shell model, Pu-238.

1. INTRODUCTION

The spontaneous emission of fragments with intermediate mass between fission products and the alpha decay was predicted in 80's [1–7]. These exotic decay modes were experimentally evidenced in 1984 [8–12]. The properties of this phenomenon resemble to that of the alpha-decay. As a direct consequence [13], later on, a fine structure in ^{14}C decay from ^{223}Ra was discovered. The energy spectrum measurements [14, 15] revealed a fine structure with an intense branch to the excited state of ^{209}Pb daughter. The best agreement between experiment and theory was obtained by considering the cluster decay as a fission process [16, 17], treated within the macroscopic-microscopic model. Furthermore, the macroscopic-microscopic approach was developed to treat in a unitary manner the cluster decay and the fission process. In this sense, a magic valley in the ^{232}U potential energy surface was evidenced recently [18,19]. This valley belongs to a mass asymmetry consistent with the formation of the ^{208}Pb. A similar valley was obtained recently within the Hartree-Fock-Bogoliubov approximation [20]. It is worth to mention that two valleys in the macroscopic-microscopic potential landscape were identified for the first time in Ref. [21]. One of these valleys corresponds to fission, while the second one, called fusion valley in Ref. [21] is related to a mass asymmetry compatible with the exis-

tence of a Pb daughter in a composite system. These two valleys are separated by a ridge. Such a valley will be confirmed for the heavy ion emission from ^{238}Pu.

2. MODEL

In the following, the calculation addresses ^{32}Si emission from ^{238}Pu. The microscopic-macroscopic model [22] is exploited dynamically, by determining the least action trajectory. The dynamical analysis of a fissioning nucleus requires at least the knowledge of the deformation energy and the effective mass. For simplicity, in the macroscopic-microscopic model one assumes that these quantities depend upon the shape coordinates. Thus, in our analysis, the basic ingredient is the nuclear shape parametrization. The nuclear shape parametrization used is given by two ellipsoids of different sizes smoothly joined by a third surface obtained by rotating a circle around the symmetry axis. Five degrees of freedom characterize this nuclear shape parametrization: the elongation, given by the inter-nuclear distance $R = z_2 - z_1$ between the centers of the ellipsoids, the two deformations of the nascent fragments denoted by their eccentricities $\epsilon_i = [1 - (b_i/a_i)^2]^{1/2}$ (i=1,2), the mass asymmetry given by the ratio of major semi-axis $\eta = a_2/a_1$ and the necking parameter related to the curvature of the intermediate surface $C = s/R_3$. The quantity C is used for swollen shapes in the median region, while R_3 is used for necked shapes. A single nucleus and two separated fragments are allowed configurations. The determination of the fission trajectory can be obtained through a minimization of the action integral in our five-dimensional configuration space, starting with the ground state of the system and ending at the exit point of the barrier or in the scission configuration. For fission, such calculations were already realized for Th, U [23–25] and Cf [26, 27].

The probability P of a given channel in a fission process is ruled by an exponential factor within the WKB approximation [28].

$$P = \exp\left\{-\frac{2}{\hbar}\int_{R_i}^{R_f}\sqrt{2(V(R,C,\epsilon_1,\epsilon_2,\eta)B\left(R,C,\epsilon_1,\epsilon_2,\eta,\frac{\partial C}{\partial R},\frac{\partial \epsilon_1}{\partial R},\frac{\partial \epsilon_2}{\partial R},\frac{\partial \eta}{\partial R}\right)}dR\right\} \quad (1)$$

The exponent of the above relation gives the classical action integral of a fixed energy along a trajectory in our multidimensional configuration space. In the present work, this energy is considered as the ground state energy of the parent nucleus. In fission, the trajectory connects the ground state configuration R_i to the exit point of the barrier R_f. In the cluster decay case, the minimization has to be performed up the configuration of two touching nuclei, denoted R_t. To this purpose, two ingredients are required: the deformation energy V and the tensor of the effective mass B.

The deformation energy V was obtained by summing the liquid drop energy

E_{LDM} with the shell and the pairing corrections δE:

$$V = E_{LDM} + \delta E. \tag{2}$$

The macroscopic energy E_{LDM} is obtained in the framework of the Yukawa - plus - exponential model [29] extended for binary systems with different charge densities [30] as detailed in [31]. The diffuseness correction to the Coulomb potential as described in [29, 32], is taken into account.

The shell effects δE are obtained as a sum between the shell δU and pairing δP corrections. In this context the Strutinsky procedure was used. These corrections represent the varying part of the total binding energy caused by the intrinsic structure. In calculating the pairing effect, constant values of the pairing matrix elements are computed separately for the parent and the two fragments. A renormalization procedure [28] in the BCS theory that depends on the energy level distribution and a smoothed gap distribution is used to obtain the values of the pairing matrix elements associated to each fragment issued in the the reaction.

The deformation energy is a function of the collective parameters, giving the generalized forces acting on the nuclear shape. For a complete description of the fission process, it is also necessary to know how the nucleus reacts to these generalized forces. This information is contained in the effective mass of the system [28]. The most used approach to calculate the inertia is the cranking model. Recently, the cranking model was generalized by taking into account the intrinsic excitation produced during the fission process itself [33]. In our investigation, three different approximations to describe the inertia are used. First of all, for the determination of the fission trajectory, the mass parameters are evaluated microscopically within the cranking model [33–35].

To calculate the inertia and the shell effects, we need a microscopic potential. The microscopic potential has to be consistent with our nuclear shape parametrization. The simplest way to define the mean field it to use a semi-phenomenological Woods-Saxon potential. In order to take into account nuclear deformations going over to separate shapes, a two-center shell model with a Woods-Saxon potential was recently developed [17]. The mean field potential is defined by the relation:

$$V_0(\rho, z) = \frac{V_c}{1 + \exp\left[\frac{\Delta(\rho,z)}{a}\right]}, \tag{3}$$

where $\Delta(\rho, z)$ is the distance between a point (ρ, z) and the nuclear surface. This distance is measured only along the normal direction on the surface and it is negative if the point is located in the interior of the nucleus. V_c is the depth of the potential, while a is the diffuseness parameter. In our work, the depth is $V_c = V_{0c}[1 \pm \kappa(N_0 - Z_0)/(N_0 + Z_0)]$ with plus sign for protons and minus sign for neutrons, $V_{0c} = 51$ MeV, a=0.67 fm, κ=0.67. Here, A_0, N_0 and Z_0 represent the mass

number, the neutron number and the charge number of the parent, respectively. The Blomqvist-Walhlborn parametrization is adopted because it provides the same constant radius r_0 for the mean field and the pairing field. It ensures a consistency of the shapes of the two fields at hyperdeformations, *i.e.*, two tangent ellipsoids. The Hamiltonian is obtained by adding the spin-orbit and the Coulomb terms to the Woods-Saxon potential. The eigenvalues are obtained by diagonalizing the Hamiltonian in the semi-symmetric harmonic two center basis [36, 37]. In this work, the maximal principal quantum number is $N_{max} = 14$. The two center Woods-Saxon model will be used to compute shell and pairing corrections together with inertia. The two center shell model represents a valuable instrument to investigate the role of individual orbitals for the treatment of a wide variety of superasymmetric disintegration processes, pertaining to cluster- and alpha-decays [16, 38–41] or superheavy elements [42, 43].

3. RESULTS AND DISCUSSION

It is not possible to directly minimize the functional (1), due to the large computing time determining the values of the potential energies and of the effective masses. Thus, in the relevant configuration space, a small number of potential energies and inertia are computed and their interpolated values are used in the minimization procedure. First of all, a grid of 691 200 deformation values was fixed in our five-dimensional configuration space: 20 values of R between 0 fm and and the scission point, 8 values of eccentricities ϵ_i between 0 and 0.75, 15 values of the ratio $\eta = a_1/a_2$ in the interval 1 and 3 and 32 values for C between -0.11 and 0.20 fm^{-1}, (5 values for R_3 between 0 and 4 fm are also added). The deformation energy and the elements of the inertia tensor were computed in these selected points. In this way, the pertinent region in the configuration space including the possible fission trajectories between the ground state and the scission configuration R_t was spanned. The quantities of interest in this selected region were obtained by interpolating the calculated masses and the energies. The interpolation was realized using spline functions. If the difference between the interpolating points is large, oscillations of the interpolated values can occur. In these cases, the oscillations are eliminated by interpolating the logarithmic values in the mesh points. The trajectory emerges by minimizing numerically the action functional, with a method initiated in [44] and used to describe fission processes [23, 24, 26, 45–49]. First of all the parent ground state and the final configuration of two tangent nuclei were identified. Several points in the configuration space, characterized by small values of the deformation energy, that connect these two configurations are used as input parameters. The trajectory is obtained as a spline (or linear) interpolation between these points. The action integral is minimized numerically. Different initial values were tested and the best trajectory is retained.

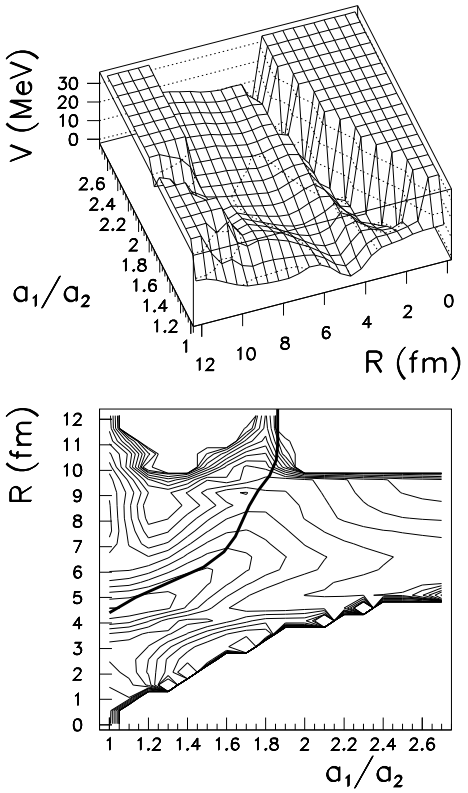

Fig. 1 – Upper part: potential energy surface V as function of the elongation R and the mass asymmetry $\eta = a_1/a_2$. Lower part. contour plot of the potential energy surface. The step between two equipotential curves is 2 MeV. The variations of the coordinates ϵ_1, ϵ_2, and C follow the least action path as function of R. The least action trajectory is plotted within a thick curve.

Due to the fact that we used interpolated values, we don't have a great confidence in this primary minimization. Therefore, the best trajectory obtained previously was tested hundreds of times by varying slowly the generalized coordinates to improve the value of the exact action integral. It is also possible to minimize the action integral by solving the associated Euler-Lagrange equations [50, 51]. Another widely used method in determining the fission path is the immersion procedure [52].

The superasymmetric fission trajectory, as well as the landscapes of the deformation energies are displayed in Figs. 1 and 2. In Fig. 1, the potential energy surface is represented as function of the mass asymmetry parameter $\eta = a_1/a_2$ and the elongation R. The dependencies of all generalized coordinates as function of R follow the variation obtained along the minimal action trajectory. The ground state of the parent nucleus is located at an elongation R=4.6 fm with a mass asymmetry $\eta \approx 1$.

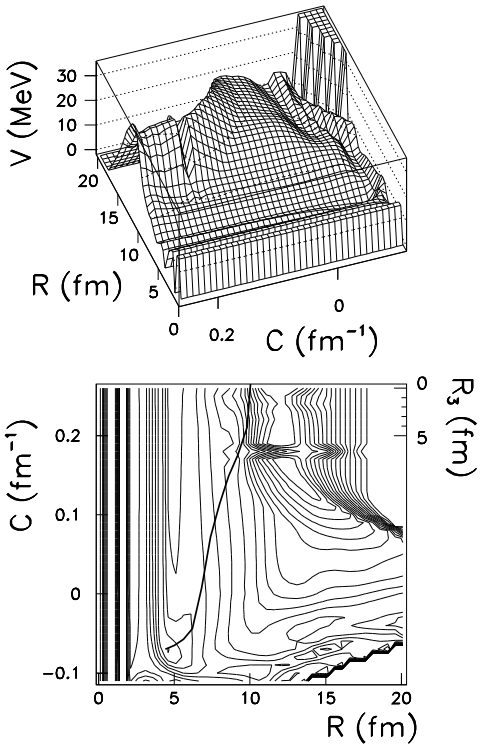

Fig. 2 – Same as Fig. 1 for a representation in the C and R generalized coordinates. For C greater that 0.2 fm^{-1} one uses the right scale for $R_3 = 1/C$. The step between two equipotential lines is 2 MeV.

The ratio a_1/a_2 abruptly changes when the nucleus stars to deform, *i.e.*, when the elongation increases. A compatible with the final mass asymmetry value is very soon obtained. It is clearly evidenced that the nuclear system follows a well behaved valley in the potential energy surface up to the scission configuration located at $R_t \approx 10$ fm. The scission configuration is approximatively described by two tangent spherical fragments. It is interesting to stress that in the case of the fission phenomena, the situation is very different. The behavior for fission is displayed for a_1/a_2 ≈1.-1.2 fm, where two fragments of comparable sized are formed. It can be seen in Fig. 1 that a double barrier occurs. The nucleus, initially in the ground state, is fissioning by penetrating a first barrier located at R=6.5-7 fm and reaches a second well at R=8 fm. The situation is completely different for the cluster decay [18]: as mentioned the system follows an energy valley in the deformation energy. When the elongation is larger than R_t, the valley in the potential energy surface is extended in the external region for the system ^{208}Pb+^{32}Si.

In Fig. 2, the deformation energy is displayed in the plane (C, R). The ground

state s located at R=4.8 fm and has a necking parameter C=0.08 fm^{-1}. So, in the ground state the shapes are swollen. These swollen shapes are preserved up to R=6 fm. From this value, the necking parameter starts to vary abruptly and the shapes become very necked producing the rupture at $R_t \approx 10$ fm. At scission, the configuration of nearly two touching nuclei is obtained.

In this paper, the ^{32}Si emission from ^{238}Pu was considered as a superasymmetric fission process and it was treated within the macroscopic-microscopic approximation. The fragmentation potential in the overlap region was obtained in conjunction with the minimal action principle. It was shown that the cluster decay follows a well behaved valley in the potential energy landscape, connected to the formation of the Pb nucleus. This behavior is in line with results published recently [20]. A new fission valley that leads to cluster decay was found within the Hartree-Fock-Bogoliubov approximation. On another hand, the cluster decay can be treated within preformation models [53], as in alpha-decay [54].

Acknowledgments. Work supported by CNCS UEFISCDI, project number PN-II-ID-PCE-2011-3-0068.

REFERENCES

1. A. Sandulescu, W. Greiner, J. Phys. G **3**, L189 (1977).
2. A. Sandulescu, H.J. Lustig, J. Hahn, W. Greiner, J. Phys. G **4**, L279 (1978).
3. A. Sandulescu, D.N. Poenaru, W. Greiner, Sov. J. Part. Nucl. **11**, 528 (1980).
4. A. Sandulescu, J. Phys. G **15**, 529 (1989).
5. A. Sandulescu, W. Greiner, Rep. Prog. Phys. **55**, 1423 (1992).
6. A. Sandulescu, D.N. Poenaru, W. Greiner, J.H. Hamilton, Phys. Rev. Lett. **54**, 490 (1985).
7. D.S. Delion, *Theory of particle and cluster emission* (Springer-Verlag, Berlin, 2010).
8. H.J. Rose, G.A. Jones, Nature **307**, 245 (1984).
9. A. Sandulescu, Yu.S. Zamyatnin, J.A. Lebedev, B.F. Myasoedov, S.P. Tretyakova, D. Hasegan, JINR Rapid Commun. **5**, 5 (1984).
10. E. Hourani, M. Hussonois, L. Stab *et al.*, Phys. Lett. B **160**, 375 (1985).
11. S. Gales, E. Hourani, M. Hussonois, H.P. Shapira, M. Vergnes, Phys. Rev. Lett. **53**, 759 (1984).
12. S.W. Barwick, P.B. Price, J.D. Stevenson, Phys. Rev. C **31**, 1984 (1984).
13. M. Greiner, W. Scheid, J. Phys. G **12**, 229 (1986).
14. L. Brillard, A.G. Elayi, E. Hourani, M. Hussonnois, J.F. Le Du, L.H. Rosier, L. Stab, C.R. Acad. Sci. Ser. II **309**, 1105 (1989).
15. M. Hussonnois, J.F. Le Du, L. Brillard, J. Dalmasso, G. Ardisson, Phys. Rev. C **43**, 2599 (1991).
16. M. Mirea, Phys. Rev. C **57**, 2484 (1998).
17. M. Mirea, Phys. Rev. C **78**, 044618 (2008).
18. M. Mirea, A. Sandulescu, D.S. Delion, Proc. Rom. Acad. Series A **12**, 203 (2011).
19. M. Mirea, A. Sandulescu, D.S. Delion, Nucl. Phys. A **870-871**, 23 (2011).
20. M. Warda, L.M. Robledo, Phys. Rev. C **84**, 044608 (2011).
21. T. Ichikawa, A. Iwamoto, P. Moller, A.J. Sierk, Phys. Rev. C **71**, 044608 (2005).

22. J.R. Nix, Ann. Rev. Nucl. Sci. **20**, 65 (1972).
23. M. Mirea, L. Tassan-Got, Cent. Eur. J. Phys. **9**, 116 (2011).
24. M. Mirea, Phys. Lett. B **680**, 316 (2009).
25. M. Mirea, Phys. Rev. C **83**, 054608 (2011).
26. M. Mirea, D.S. Delion, A. Sandulescu, Phys. Rev. C **81**, 044317 (2010).
27. M. Mirea, D.S. Delion, A. Sandulescu, Rom. J. Phys. **55**, 309 (2010).
28. M. Brack, J. Damgaard, A.S. Jensen, H.C. Pauli, V. M. Strutinsky, Rev. Mod. Phys. **44**, 320 (1972).
29. K.T.R. Davies, J.R. Nix, Phys. Rev. C **14**, 1977 (1976).
30. D.N. Poenaru, M. Ivascu, D. Mazilu, Comp. Phys. Commun. **19**, 205 (1980).
31. M. Mirea, O. Bajeat, F. Clapier, F. Ibrahim, A.C. Mueller, N. Pauwels, J. Proust, Eur. Phys. J. A **11**, 59 (2001).
32. P. Moller, J.R. Nix, W,D. Myers, W.J. Swiatecki, At. Data and Nucl. Data Tabl. **59**, 185 (1995).
33. M. Mirea, R.C. Bobulescu, J. Phys. G **37**, 055106 (2010).
34. M. Mirea, Rom. Rep. Phys. **63**, 676 (2011).
35. M. Petre, R.C. Bobulescu, C. Petre and M. Mirea, Rom. J. Phys. **55**, 741 (2010).
36. M. Mirea, Nucl. Phys. A **780**, 13 (2006).
37. M. Mirea, Phys. Rev. C **54**, 302 (1996).
38. M. Mirea, Phys. Rev. C **63**, 034603 (2001).
39. M. Mirea, Eur. Phys. J. A **4**, 335 (1999).
40. M. Mirea, F. Clapier, Europhys. Lett. **40**, 509 (1997).
41. M. Mirea, Mod. Phys. Lett. A **18**, 1809 (2003).
42. P. Stoica, Rom. Rep. Phys. **63**, 76 (2011).
43. M. Mirea, D.S. Delion, A. Sandulescu, Europhys. Lett. **85**, 12001 (2009).
44. D.N. Poenaru, M. Mirea, W. Greiner, I. Cata, D. Mazilu, Mod. Phys. Lett. A **5**, 2101 (1990).
45. M. Mirea, L. Tassan-Got, C. Stephan, C.O. Bacri, Nucl. Phys. A **735**, 21 (2004).
46. I. Companis, M. Mirea and A. Isbasescu, Rom. J. Phys. **56**, 63 (2011).
47. M. Mirea, L. Tassan-Got, C. Stephan, C.O. Bacri, P. Stoica, R.C. Bobulescu, J. Phys. G **31**, 1165 (2005).
48. M. Mirea, L. Tassan-Got, C. Stephan, C.O. Bacri, R.C. Bobulescu, Europhys. Lett. **73**, 705 (2006).
49. M. Mirea, L. Tassan-Got, C. Stephan, C.O. Bacri, R.C. Bobulescu, Phys. Rev. C **76**, 064608 (2007).
50. M. Mirea, D.N. Poenaru, W. Greiner, Nuovo Cimento A **105**, 571 (1992).
51. M. Mirea, D.N. Poenaru, W. Greiner, Z. Phys. A **349**, 39 (1994).
52. P. Moller, A.J. Sierk, T. Ichikawa, A. Iwamoto, R. Bengtsson, H. Uhrenholt, S. Aberg, Phys. Rev. C **79**, 064304 (2009).
53. R.G. Lovas, R.J. Liotta, A. Insolia, K. Varga, D.S. Delion, Phys. Rep. **294**, 265 (1989).
54. I. Silisteanu, A. I. Budaca, and A. O. Silisteanu, Rom. J. Phys. **55**, 1088 (2010); A. I. Budaca, I. Silisteanu, Rom. Rep. Phys. **63**, 1147 (2011); I. Silisteanu, M. Rizea, B. I. Ciobanu *et al.*, Rom. J. Phys. **53**, 1191 (2008).